Acta Biochim Biophys Sin 2026, 58(6): 1273–1280
https://cstr.cn/32197.14.abbs.2026020
https://doi.org/10.3724/abbs.2026020
Original Article

Original Article

Structural basis for the conformational changes of insulin receptor induced by three different hormone ligands

Xi Zhang[1,†], Ting Zhang[1,†], Cang Wu[2,†], Yuanzhu Gao[3,†], Shuo Zhang[4,†], Zhenglin Li[2], Linshan Zhong[1], Chenyu Xia[2], Liuqing Yang[1], Fengquan Dong[5,*], Qing Shu[6,*], Yang Fu[1,*], and Renhong Yan[1,*]

[1]Department of Biochemistry, SUSTech Homeostatic Medicine Institute, School of Medicine, Key University Laboratory of Metabolism and Health of Guangdong, Institute for Biological Electron Microscopy, Southern University of Science and Technology, Shenzhen 518055, China, [2]Department of Biology, School of Life Sciences, Southern University of Science and Technology, Shenzhen 518055, China, [3]Cryo-EM Centre, Southern University of Science and Technology, Shenzhen 518055, China, [4]School of Life Sciences, Zhengzhou University, Zhengzhou 450001, China, [5]Cardiovascular Medicine, Shenzhen University General Hospital, Shenzhen 518055, China, and [6]Department of Gastroenterology, The First Affiliated Hospital of Shenzhen University, Shenzhen People's Second Hospital, Shenzhen 518000, China

[†]These authors contributed equally to this work.

*Correspondence address. E-mail: Fengquan.dong@foxmail.com (F.D.); sq6060@163.com (Q.S.); fuy@sustech.edu.cn (Y.F.); yanrh@sustech.edu.cn (R.Y.)

Received 30 November 2025 Accepted 19 January 2026 Published 11 February 2026

Abstract

The insulin receptor (IR) is central to the regulation of glucose and lipid metabolism. Although insulin is its primary ligand, insulin-like growth factors I and II (IGF-I and IGF-II) also engage IR, albeit with reduced affinity. The structural basis of cooperative ligand binding, however, has remained poorly understood. Here, we report cryo-Electron Microscopy (cryo-EM) structures of IR in complex with insulin, IGF-I, and IGF-II, revealing that all three ligands engage the receptor at overlapping binding sites and can induce a conserved T-shaped quaternary assembly involving four ligand molecules at site 1/1′ and site 2/2′. Despite this shared overall architecture, distinct ligand-specific conformational changes are observed. Notably, IGF-I and IGF-II adopt different binding sequence at site 1 and site 2 compared to insulin, suggesting unique interaction dynamics. These structural insights highlight divergent mechanisms of ligand recognition and cooperative binding, providing a deeper understanding of hormone-induced conformational modulation of the IR.

Key words insulin receptor, IGF-I, IGF-II, cryo-electron microscopy

Introduction

The insulin receptor (IR) is a transmembrane receptor tyrosine kinase (RTK) that plays a fundamental role in regulating glucose and lipid homeostasis in humans, particularly by mediating insulin-dependent signaling pathways that control glucose uptake, metabolism, and storage in key tissues such as muscle, fat, and liver cells [1–5]. Dysregulation of IR signaling is associated with metabolic disorders including type 2 diabetes mellitus and insulin resistance syndromes, making IR a critical therapeutic target [1,3,4].

Research suggests that the IR dimer comprises two identical protomers (protomer A and protomer B), each composed of α- and β-subunits linked by disulfide bonds and exhibiting a Λ-shaped symmetric structure [6–8]. Upon insulin binding to the extracellular domain (ECD) of IR, the signal is transmitted through the transmembrane domain to the intracellular domain, inducing phosphorylation of the tyrosine kinase domain (TK) [7–11]. Insulin binds IR at two primary interaction sites, the site 1 and site 2, each present on both protomers, resulting in a total of four potential ligand-binding sites per receptor dimer (site 1/1′ and site 2/2′). Cryo-EM studies have revealed both asymmetric (*T*-shaped) and symmetric (T-shaped) conformations of IR in complex with insulin, corresponding to partially and fully active signaling states, respectively [10,11].

In addition to insulin, IR can also bind insulin-like growth factors I and II (IGF-I and IGF-II), although these interactions occur with lower affinity [12]. Recent reviews have comprehensively summar-

© The Author(s) 2026. This is an open access article distributed under the terms of the Creative Commons Attribution License (https://creativecommons.org/licenses/by/4.0/).

ized advances in the structural and biochemical understanding of insulin and IGF receptor activation mechanisms [13,14], highlighting the conserved architecture of the insulin/IGF signaling axis. However, the molecular basis of ligand recognition and cooperative binding, particularly for IGF-I and IGF-II interaction with IR, remains incompletely understood. IGF-I and IGF-II share high sequence and structural similarity with insulin and act primarily through their cognate receptors, IGF-IR and IGF-IIR, respectively [15–19] (Supplementary Figure S1). However, their capacity to engage IR, particularly the IR-A isoform, which lacks exon 11 and is frequently expressed in fetal tissues and cancer, suggests potential physiological and pathological roles in modulating IR activity, remains unclear [20–23]. Despite extensive structural studies have elucidated IR-insulin complexes and, more recently, IGF-II bound IR structures, establishing a general framework for receptor activation [24,25], how IGF-I and IGF-II bind to full-length IR-A and induce cooperative or distinct conformational changes remains largely unexplored.

To address this gap, we determined cryo-EM structures of full-length human IR-A bound to insulin, IGF-I, and IGF-II. While insulin- and IGF-II-bound IR structures have been characterized previously [25], the molecular basis of IGF-I recognition by full-length IR-A has remained elusive. Previous structural information was limited to an IR-B/IGF-1R hybrid receptor, in which a single IGF-I molecule occupies site 1 [26]. Here, we present the first cryo-EM structures of full-length IR-A in complex with IGF-I, revealing that IR-A can accommodate up to four IGF-I molecules at sites 1/1′ and 2/2′. Taken together, these data uncover ligand-dependent local conformational differences and provide a structural framework for understanding ligand-specific IR activation and cooperativity.

Materials and Methods

Protein expression and purification

Full-length human IR-A (accession number: NM_001079817.3) with 3× Flag-Affinity Tag at the C-terminal tail was subcloned into the pCDNA3.1 expression vector (Lab-preserved). The receptor was expressed by HEK293F cells (Sino Biological, Beijing, China) that were grown at 37°C in SMM-293T-II expression medium (Sino Biological). When the cell density reached to 2–3 × 10^6 cells/mL, the cells were transiently transfected with 1 mg/L endotoxin-free plasmid [mixed with polyethyleneimine, 1:3 (w/w) ratio], maintained for 72 h at 30°C, and harvested by centrifugation at 1500 *g* for 3 min. The cells were resuspended in lysis buffer containing 25 mM Tris-HCl pH 8.0, 200 mM NaCl, 1.0% (w/v) DDM (ndodecyl-b-D-maltopyranoside; APExBIO, Houston, USA), and protease inhibitor cocktail (APExBIO) and harvested by centrifugation at 100,000 *g* for 1 h. The supernatant was collected and incubated with anti-DYKDDDDK affinity beads (Smart-Lifesciences, Beijing, China) and then washed with more than 10 column volumes of washing buffer [PBS buffer with 0.1% (w/v) DDM and 1× protease inhibitor cocktail]. Finally, the targeted protein was eluted by 0.2 mg/mL Flag peptides and further purified by size exclusion chromatography (Superose 6 10/300 GL; Cytiva, Marlborough, USA) in PBS buffer with 0.03% (w/v) DDM. For cryo-EM sample preparation, the IR protein was mixed with Amphipol A8-35 at 1:5 (w/w) with gentle rotation for approximately 12 h, and then Bio-Beads SM-2 (Bio-Rad, Hercules, USA) was added to remove superfluous detergent. Finally, the Bio-Beads were removed by centrifugation, and the protein was further purified by a Superose 6 increase 10/300 GL size-exclusion column. Insulin (Sigma-Aldrich, St Louis, USA), IGF-I (GroPep, Adelaide, Australia) and IGF-II (GroPep) dry powder were dissolved and further purified by size-exclusion chromatography with PBS buffer.

EM data acquisition, model building and refinement

A 3 μL concentrated samples (IR:insulin/IGF-I/IGF-II, with a molar ratio of 1:1–6) were added to the glow-discharged Quantifoil R1.2/1.3 300-mesh gold holey carbon grids (Quantifoil, Jena, Germany). Grids were waited for 3.0 s and blotted for 3.0 s under 100% humidity at 4°C before being plunged into liquid ethane by a Vitrobot (FEI). Micrographs were acquired on a Titan Krios microscope (FEI) operated at 300 kV with a K3 Summit direct electron detector (Gatan, Pleasanton, USA), yielding a pixel size of 0.66 Å on images. The defocus range was set from –1.0 to –2.5 mm. Each micrograph was dose-fractionated to 32 frames under a dose rate of 20 e^-/pixel/s, with a total exposure time of 1.08 s. All steps of image processing were performed using cryoSPARC software tools [27,28] (Supplementary Figures S2–S9). All resolutions were estimated by applying a soft mask around the protein density using the gold-standard Fourier shell correlation (FSC, 0.143) [29]. Models from the AlphaFold2AF-P06213-F1-model_v4.pdb and previously reported structures (PDB: 5U8Q, 6PXW, 6VWG, and 6PXV) were initiated by docking each domain derived into the cryo-EM map by UCSF ChimeraX software, further adjusted in Coot [30–32]. Finally, the model was refined by Phenix software [33].

Results

Cryo-EM structures of the IR bound to different hormones

To elucidate the structural basis of IGF-I binding to the IR, we performed single-particle cryo-EM analysis of full-length IR in the presence of saturating concentrations of IGF-I, using molar ratios of 1:6 and 1:12 (IR:IGF-I). These datasets revealed multiple conformational states, with three or four IGF-I molecules bound. By combining particles from both conditions, we obtained four distinct reconstructions at resolutions of 3.24 Å, 3.53 Å, 5.00 Å, and 3.31 Å, enabling detailed structural analysis (Figure 1 and Supplementary Figures S3 and S4).

To capture lower-occupancy states, we also analyzed IR in the presence of reduced IGF-I concentrations (1:3 molar ratio). Across all tested conditions, two predominant conformations consistently emerged: an asymmetric state with two IGF-I molecules bound, and a symmetric T-shaped state with four IGF-I molecules bound (Supplementary Figure S4). In the asymmetric conformation, IGF-I molecules occupy binding site 1 and site 2 on protomer A, while site 1′ and site 2′ on protomer B remain unoccupied, resulting in increased flexibility in the CR–L1 domains of protomer A and the FnIII-1 to -3 domains of protomer B (Figure 1). In contrast, the symmetric T-shaped conformation displays all four IGF-I molecules bound at site 1/1′ and site 2/2′, stabilizing the extracellular domains (Supplementary Figure S8).

We next investigated the interaction between IR and IGF-II, a structurally homologous ligand of IGF-I. Cryo-EM analysis of IR in complex with IGF-II at a 1:6 molar ratio revealed two main conformations: an asymmetric state with two IGF-II molecules (3.35 Å, predominant class) and a symmetric T-shaped conformation with four IGF-II molecules (approximately 8 Å). Although the latter exhibited lower resolution, IGF-II densities near the FnIII-1

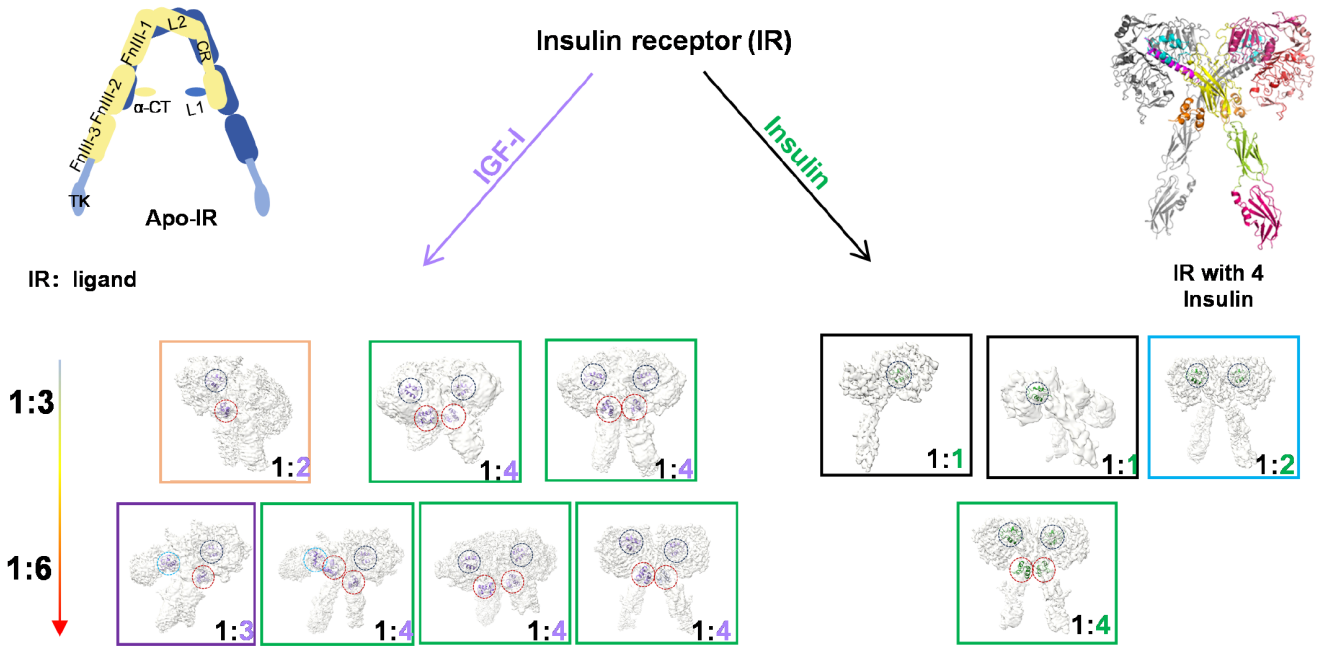


Figure 1. Cryo-EM structures of the IR bound to insulin or IGF-I across a ligand concentration series Representative reconstructions illustrate different ligand-occupancy states of the IR dimer obtained under increasing concentrations of insulin or IGF-I. The occupancy label (*e.g.*, 1:2, 1:3, 1:4) denotes the number of bound ligands per IR dimer in the corresponding structure.

domains were clearly discernible (Supplementary Figure S7). These conformations were largely consistent with those observed in the IR/IGF-I complex (Supplementary Figures S3 and S4). Interestingly, in the asymmetric IR/IGF-II structure, the FnIII-3/FnIII-3′ domains showed tight inter-protomer contacts, differing from a recently reported structure (Supplementary Figure S10). Attempts to capture lower-occupancy states at reduced IGF-II concentrations were unsuccessful, suggesting that IGF-II preferentially stabilizes asymmetric *T*-shaped states over the symmetric T-shaped conformation.

To directly compare ligand-induced binding patterns, we also determined the cryo-EM structures of IR in complex with insulin at molar ratios of 1:3 and 1:6 under identical experimental conditions (Figure 1 and Supplementary Figures S5 and S6). As expected, increasing insulin concentrations correlated with greater ligand occupancy, resulting in three predominant conformational states: IR bound to one, two, or four insulin molecules (Supplementary Figure S9). At low insulin concentrations (1:3), a T-shaped conformation with insulin bound only to site 1 and site 1′ was readily detected (Supplementary Figure S6). In contrast, under saturating conditions, only the fully active T-shaped conformation with four insulin molecules bound was observed, consistent with previous reports (Supplementary Figure S5) [10]. Notably, in the singly bound IR-insulin structure, significant flexibility was observed in the FnIII-2′ and FnIII-3′ domains of protomer B. In contrast, the T-shaped conformations with two or four insulin molecules exhibited comparable overall architectures, representing fully active states of the receptors (Supplementary Figure S9) [11].

A comparative analysis of ligand binding sequences revealed distinct ligand-specific dynamics. For IGF-I, occupation of site 1 is followed by binding at site 2, with subsequent engagement of site 1′ and site 2′ at higher ligand concentrations. This binding order contrasts with that of insulin, which has been proposed to initially engage site 2′ in the membrane-proximal FnIII-1′ domain before transitioning to site 1 formed by the L1 domain, α-CT′, and FnIII-1′, as proposed by Nielsen *et al.* [34]. Similarly, IR bound to IGF-II at a 1:6 molar ratio exhibited two structural states, one with IGF-II molecules occupying site 1 and site 2, and another with all four sites occupied, suggesting a binding sequence analogous to that of IGF-I (Supplementary Figures S7 and S10). These ligand-specific binding behaviors likely contribute to their divergent physiological roles and downstream signaling outputs [4,19].

Interaction interfaces for different hormones at binding site 1

To elucidate the molecular determinants underlying hormone recognition by the IR, we focused on the detailed interaction interfaces at binding site 1, a critical region that initiates ligand-induced conformational changes. In contrast, binding site 1′ and site 2/2′ exhibited relatively weak ligand densities (Supplementary Figures S8–S10), highlighting the central role of site 1 in hormone engagement.

At binding site 1, a composite binding pocket is formed by three structural elements: the L1 domain from protomer A, the α-CT′ helix, and the FnIII-1′ domain from protomer B. Together, these elements delineate a binding cavity composed of at least 20 interface residues that accommodate hormone molecules [11]. In the IR/insulin complex, key residues contributing to the binding pocket include Asn42, Glu61, and Lys148 from the L1 domain; Arg744, Glu733, and Glu738 from the α-CT′ helix; and Asn568 from the FnIII-1′ domain. For the IR/IGF-I complex, the pocket is formed by Asn42, Arg41, and Glu343 from the L1 domain; Asn738 and Arg744 from the α-CT′ helix; and Arg566 from the FnIII-1′ domain. Similarly, in the IR/IGF-II complex, the binding pocket comprises Asn42, Lys67, and Gly37 from the L1 domain; Arg744 and Glu738 from the α-CT′ helix; and Pro522 from the FnIII-1′ domain (Figure 2A–C).

Notably, Arg744 and Glu738 of the α-CT′ helix, together with Asn42 from the L1 domain, are consistently involved in binding all three hormones, indicating a conserved recognition mechanism at

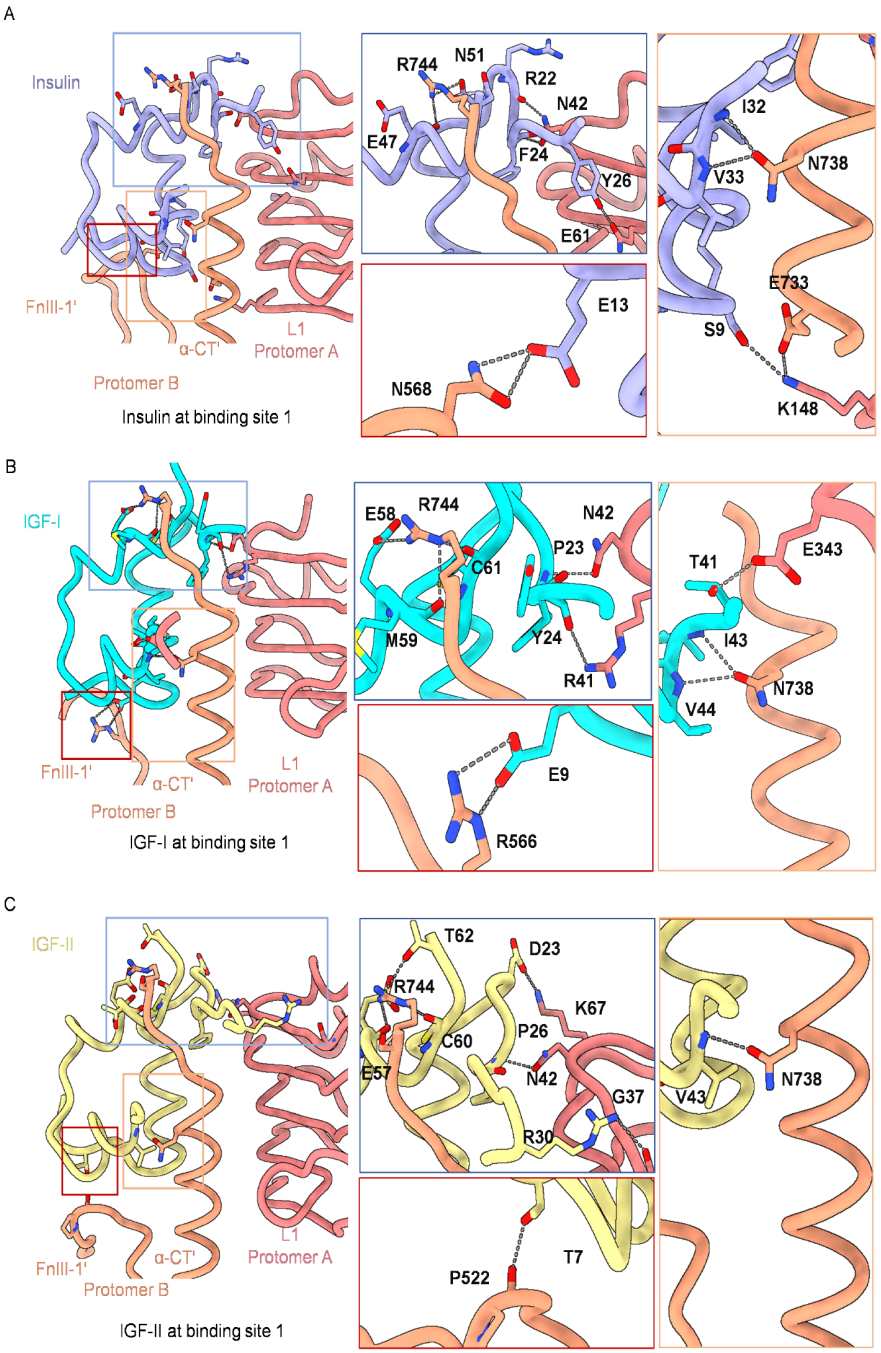


Figure 2. Interaction interfaces for different hormones at binding site 1 The insulin, IGF-I and IGF-II are colored as light purple, cyan and yellow, while the protomer A and protomer B are marked as light orange and light red, respectively.

site 1. Among the tested ligands, insulin demonstrated the highest binding affinity, as reflected by the greater number of hydrogen bonds formed, which is consistent with previous observations [15].

The conformational changes of the IR/IGF-I and IR/insulin complexes

We next examined the overall conformational changes of the IR upon IGF-I binding. Notably, the transient occupancy of binding site 1/2, an interface between sites 1 and 2, by a third and fourth IGF-I molecule introduces substantial flexibility to surrounding domains prior to the establishment of the canonical T-shaped conformation (Figure 3). This increased flexibility is particularly evident in the FnIII-1, FnIII-2, and FnIII-3 domains of protomer A, as well as the L1 domain of protomer B, all of which undergo marked shifts despite the inherent symmetry of the IR dimer (Figure 3).

In contrast, the IR-insulin complex exhibits greater conformational stability across different ligand-bound states. Specifically, the L1, CR, and L2 domains of protomer A, together with the α-CT′ helix and FnIII-1′ domain of protomer B, remain largely unaltered upon binding one, two, or four insulin molecules, owing to insulin's high-

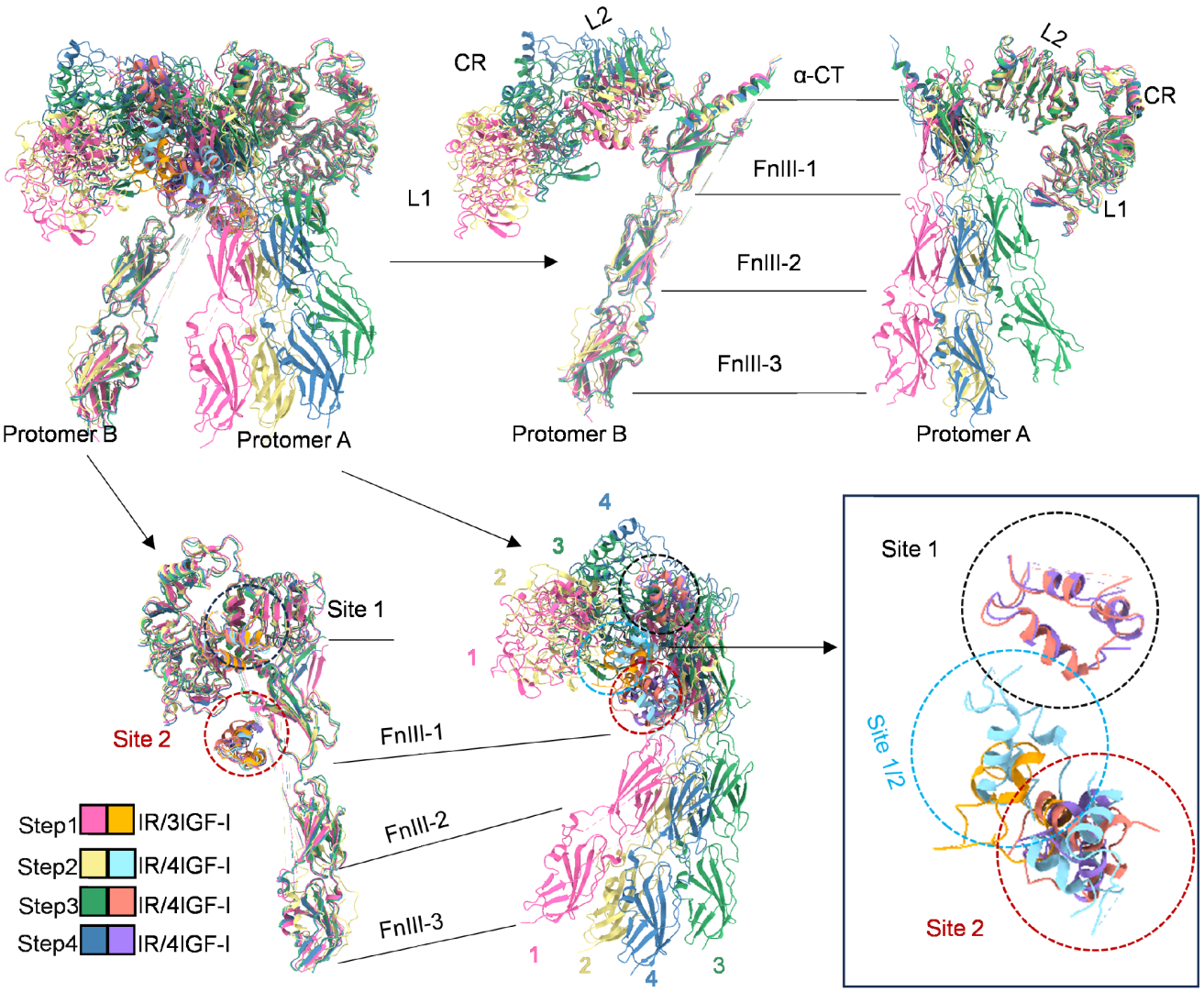


Figure 3. Structural comparison of IR-IGF-I complexes in different conformational states Protomer A and protomer B of the IR dimer are indicated in all panels. The IR protomers are shown in pink, yellow, green, and dark blue, respectively, while the corresponding bound IGF-I molecules are colored orange, cyan, salmon, and purple. Structural superposition of IR-IGF-I complexes reveal a series of distinct conformational states of the receptor associated with increasing ligand occupancy. Based on these structures, a putative conformational progression is proposed. Step 1, one IGF-I molecule is observed at the site 1/2 region. Steps 2–3, two IGF-I molecules bind at distinct positions corresponding to site 1 and site 2, accompanied by local rearrangements of the αCT helix and the FnIII-1 domain of protomer B. Step 4, the extracellular "head" region (L1, CR, L2, FnIII-1, αCT helix, and IGF-I) becomes stabilized, while the relative flexibility of the FnIII-2 and FnIII-3 domains of protomer B is reduced.

affinity engagement at binding site 1 (Figure 4).

We further compared the fully ligand-bound T-shaped conformations of the IR/IGF-I and IR/insulin complexes. Overall, the symmetric structures are highly similar, particularly in the head region encompassing the L1, CR, L2, FnIII-1 domains and α-CT helix. However, when aligned by protomer A, clear differences emerge in the relative positioning of the two FnIII domains, especially in their interdomain distances (Supplementary Figure S11).

Interestingly, we did not observe any structures of IR bound with two IGF-I or IGF-II molecules both occupying binding site 1 and site 1′. Instead, an asymmetric conformation was consistently observed, wherein the two hormone molecules occupy binding sites 1 and 2 of protomer A, even at a 1:3 ligand-to-receptor ratio. These findings suggest hormone-specific conformational dynamics during IR activation, pointing to distinct mechanisms of receptor engagement and activation by insulin, IGF-I, and IGF-II, which may underlie their differential physiological functions.

Discussion

Insulin-like growth factors are secreted at relatively stable levels, in contrast to the rapid and transient fluctuations of insulin. Consistent with this physiological difference, our structures show that the predominant conformations of the IR/IGF-I complex remain largely unchanged across varying ligand concentrations. This concentration-independent behavior suggests that IGF-I promotes a more sustained and stable mode of receptor activation, potentially supporting long-term cellular functions such as growth, differentiation, and metabolism, rather than acute regulation of glucose homeostasis.

It should be emphasized that the cryo-EM structures presented

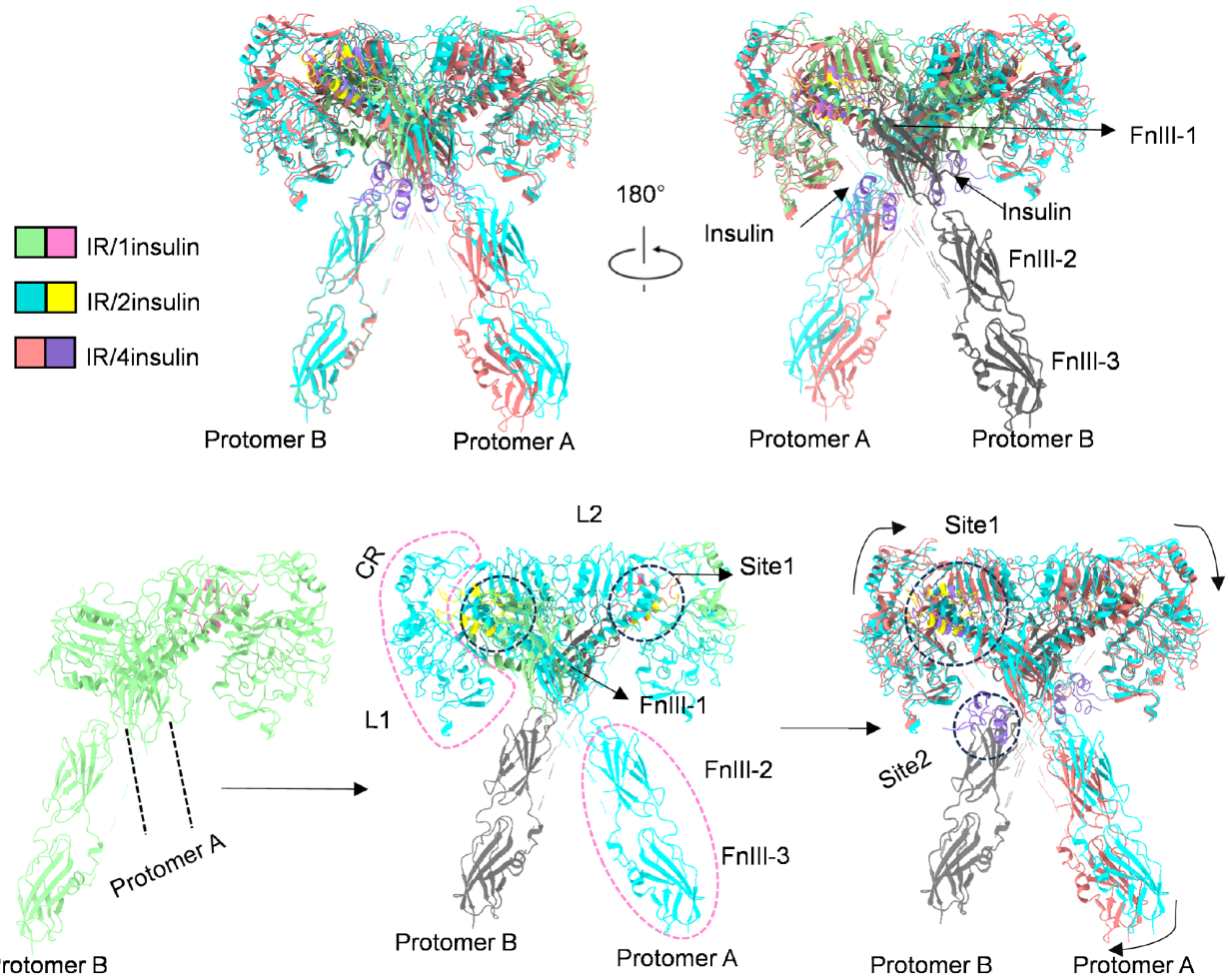


Figure 4. Conformational changes of IR in complex with insulin The IR dimers are shown in light green, cyan, and salmon, with the corresponding bound insulin molecules colored pink, yellow, and purple, respectively. Regions showing minimal conformational changes among these insulin-bound states, including FnIII-1, FnIII-2, and FnIII-3, are shown in gray. During the transition from the one-insulin to the two-insulin occupancy state, regions undergoing notable conformational rearrangements are highlighted by pink boxes. In the four-insulin bound state, both protomer A and protomer B undergo coordinated movements, resulting in a more stabilized overall receptor conformation.

here were obtained under *in vitro* conditions using elevated ligand concentrations to stabilize distinct receptor-bound states. These structures therefore define the conformational space accessible to the insulin receptor upon ligand engagement, rather than representing the dominant signaling states under physiological conditions.

By comparison, the canonical *T*-shaped conformation of the IR/insulin complex is only stabilized under saturating insulin conditions, reflecting a concentration-dependent mechanism that aligns with the rapid and tightly regulated demands of glucose homeostasis. Although the overall assemblies of IR bound to insulin, IGF-I, IGF-II, and insulin-like polypeptides appear similar, their dynamic conformational transitions differ in a ligand-specific manner [25,35,36].

An intriguing finding is that IGF-I can occupy all four receptor binding sites more readily than insulin, despite insulin having a higher overall binding affinity for IR. This apparent paradox may be explained by differential site specific affinities, particularly at binding site 1′ and 2. Previous biochemical studies have established that insulin receptor activation involves two spatially distinct but functionally coupled binding surfaces and exhibits pronounced negative cooperativity, such that differences in site-specific engagement can substantially influence ligand occupancy and conformational outcomes [37]. Moreover, recent structural and functional analyses have suggested that insulin and IGF ligands differ in their reliance on site-2 engagement, providing a mechanistic basis for ligand-specific cooperativity and activation pathways [25]. Our structural data suggest that IGF-I binds to site 1 and site 2 more efficiently than insulin, facilitating the formation of fully occupied symmetric conformations even at lower ligand concentrations. Based on these findings, we propose a dynamic combinatorial binding model to account for the ligand-specific occupancy patterns and conformational transitions of IR upon binding insulin, IGF-I, or IGF-II (Figure 5). This model highlights the importance of individual binding site affinities and local flexibility in shaping the overall activation mechanism of the receptor.

Comparison with previously reported insulin receptor complexes further contextualizes our findings. The insulin-bound structures [10,11] and the IGF-II:IR-B complexes [25] collectively revealed conserved features of ligand-induced activation, while the hybrid IR-B/IGF-1R:IGF-I structures [26] demonstrated that IGF-I engages only a single site on the hybrid receptor. Our full-length IR-A:IGF-I

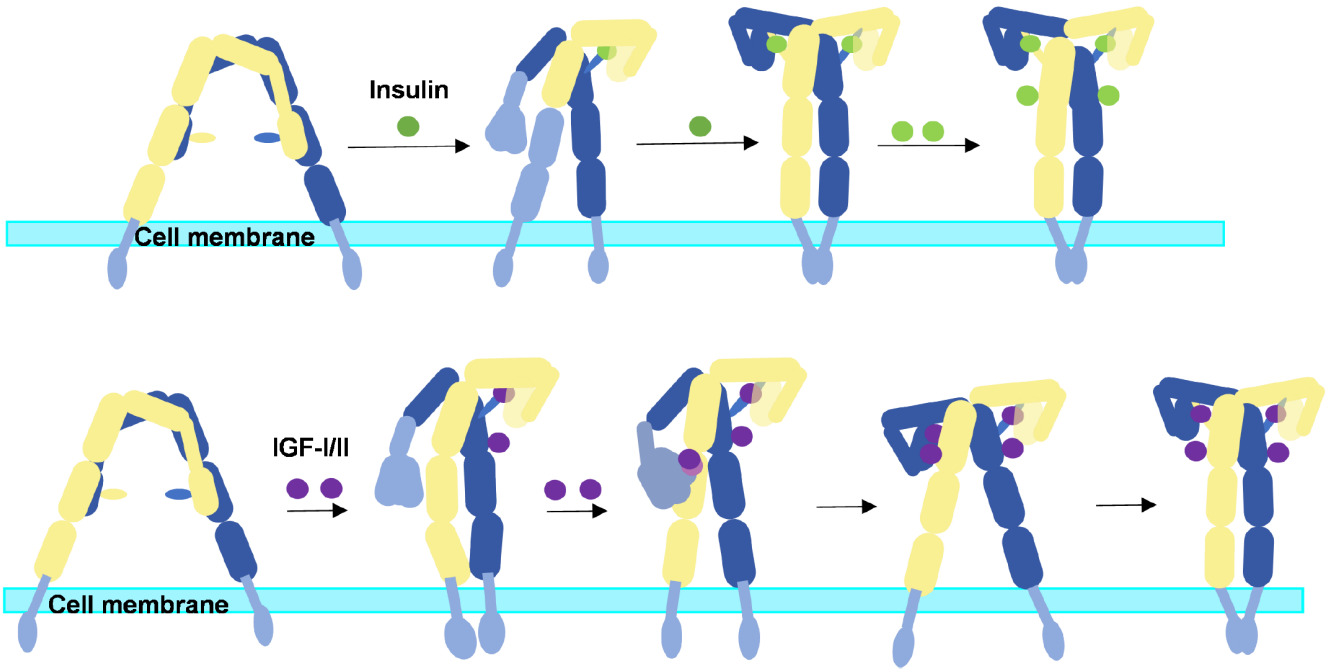


Figure 5. The working models of how different hormone ligands bind to IR Schematic models summarize the proposed activation of IR upon binding insulin or insulin-like growth factors (IGF-I/IGF-II). Insulin and IGFs are shown as green and purple spheres, respectively. The light-blue region indicates flexible parts with lower local resolution in the cryo-EM reconstructions.

structures extend these observations by showing multi-ligand occupancy and a distinct mode of cooperative activation not previously observed for IGF ligands.

These results, together with the binding sequence model proposed by Nielsen *et al.* [34] and the comprehensive structural perspectives summarized in [13,14], provide an integrated view of ligand recognition within the insulin receptor family. Collectively, this study advances our understanding of how insulin, IGF-I, and IGF-II differentially modulate IR activation and signaling specificity.

Supplementary Data

Supplementary data are available at *Acta Biochimica et Biophysica Sinica* online.

Acknowledgement

We thank Drs Shuman Xu, Lei Zhang, Yuanzhu Gao, and Peiyao Li at the Cryo-EM Center of SUSTech for technical support in electron microscopy data acquisition. Renhong Yan is an investigator of SUSTech Institute for Biological Electron Microscopy.

Data Availability

Atomic coordinates and cryo-EM density maps of the IR/IGF-I complexes (PDB: 8XJS, whole map: EMD-38404; PDB: 8XK1, whole map: EMD-38413; PDB: 8XKR, whole map: EMD-38423; PDB: 8XKM, whole map: EMD-38420), the IR/insulin complexes (PDB: 8YYL, whole map: EMD-39675; PDB: 8YYS, whole map: EMD-39677; PDB: 8YYT, whole map: EMD-39678), and the IR/IGF-II complexes (PDB: 8YSZ, whole map: EMD-39566) have been deposited to the Protein Data Bank (http://www.rcsb.org) and the Electron Microscopy Data Bank (https://www.ebi.ac.uk/pdbe/emdb/), respectively (Supplementary Table S1). And all maps and coordinates are available from the corresponding authors upon reasonable request.

Funding

This work was mainly supported by the grants from the National Natural Science Foundation of China (No. 32422039 to R.Y.), the Shenzhen Science and Technology Program (No. RCYX20231211090342048 to R.Y.), the Shenzhen Medical Research Fund (Nos. A2303046 and B2402043 to R.Y.), the Major Talent Recruitment Program of Guangdong Province (No. 2021QNO2Y167 to R.Y.), the Medical Scientific Research Foundation of Guangdong Province of China (No. A2021333 to F.Q.D.), Shenzhen Science and Technology Innovation Commission Project (No. JCYJ20190808120613189 to F. Q.D.), Shenzhen science and technology research and development fund project (No. KCXFZ20201221173208023-1039027 to Q.S.), the Shenzhen Pea-cock Team Project (No. KQTD20200909113758004 to Y.F.). And Special thanks to the support of Taidu Biotech (Suzhou) Co., Ltd. in protein purification equipments.

Conflict of Interest

The authors declare that they have no conflict of interest.

References

1. Kasuga M, Karlsson FA, Kahn CR. Insulin stimulates the phosphorylation of the 95,000-Dalton subunit of its own receptor. *Science* 1982, 215: 185–187
2. Ebina Y, Ellis L, Jarnagin K, Edery M, Graf L, Clauser E, Ou J, *et al.* The human insulin receptor cDNA: the structural basis for hormone-activated transmembrane signalling. *Cell* 1985, 40: 747–758
3. Zhang X, Zhu X, Bi X, Huang J, Zhou L. The insulin receptor: an important target for the development of novel medicines and pesticides. *Int J Mol Sci* 2022, 23: 7793
4. Lawrence MC. Understanding insulin and its receptor from their three-

dimensional structures. *Mol Metab* 2021, 52: 101255
5. Wei, Lu, Yao, Hong, Yang, Zhang, Yin, ***et al***. Insight into Janus kinases specificity: from molecular architecture to cancer therapeutics. *MedComm–Oncology* 2024, 3: e69
6. McKern NM, Lawrence MC, Streltsov VA, Lou MZ, Adams TE, Lovrecz GO, Elleman TC, ***et al***. Structure of the insulin receptor ectodomain reveals a folded-over conformation. *Nature* 2006, 443: 218–221
7. Xiong X, Blakely A, Kim JH, Menting JG, Schäfer IB, Schubert HL, Agrawal R, ***et al***. Symmetric and asymmetric receptor conformation continuum induced by a new insulin. *Nat Chem Biol* 2022, 18: 511–519
8. Li J, Park J, Mayer JP, Webb KJ, Uchikawa E, Wu J, Liu S, ***et al***. Synergistic activation of the insulin receptor via two distinct sites. *Nat Struct Mol Biol* 2022, 29: 357–368
9. Choi E, Bai XC. The activation mechanism of the insulin receptor: a structural perspective. *Annu Rev Biochem* 2023, 92: 247–272
10. Uchikawa E, Choi E, Shang G, Yu H, Bai X. Activation mechanism of the insulin receptor revealed by cryo-EM structure of the fully liganded receptor–ligand complex. *eLife* 2019, 8: e48630
11. Scapin G, Dandey VP, Zhang Z, Prosise W, Hruza A, Kelly T, Mayhood T, ***et al***. Structure of the insulin receptor-insulin complex by single-particle cryo-EM analysis. *Nature* 2018, 556: 122–125
12. Firth SM, Baxter RC. Cellular actions of the insulin-like growth factor binding proteins. *Endocrine Rev* 2002, 23: 824–854
13. Van-Duyne, Blair, Sprenger, Moiseenkova-Bell, Plymate, Penning. The androgen receptor. *Vitam Horm* 2023, 123: 439–481
14. Forbes. The three-dimensional structure of insulin and its receptor. *Vitam Horm* 2023, 123: 151–185
15. Morrione A, Valentinis B, Xu S, Yumet G, Louvi A, Efstratiadis A, Baserga R. Insulin-like growth factor II stimulates cell proliferation through the insulin receptor. *Proc Natl Acad Sci USA* 1997, 94: 3777–3782
16. Hawkes C, Kar S. The insulin-like growth factor-II/mannose-6-phosphate receptor: structure, distribution and function in the central nervous system. *Brain Res Rev* 2004, 44: 117–140
17. Kasprzak A. Insulin-Like growth factor 1 (IGF-1) signaling in glucose metabolism in colorectal cancer. *Int J Mol Sci* 2021, 22: 6434
18. Zhu Y, Chen L, Song B, Cui Z, Chen G, Yu Z, Song B. Insulin-like Growth Factor-2 (IGF-2) in Fibrosis. *Biomolecules* 2022, 12: 1557
19. LeRoith D, Holly JMP, Forbes BE. Insulin-like growth factors: ligands, binding proteins, and receptors. *Mol Metab* 2021, 52: 101245
20. Escribano O, Beneit N, Rubio-Longás C, López-Pastor AR, Gómez-Hernández A. The role of insulin receptor isoforms in diabetes and its metabolic and vascular complications. *J Diabetes Res* 2017, 2017: 1–12
21. Vella V, Giuliano M, La Ferlita A, Pellegrino M, Gaudenzi G, Alaimo S, Massimino M, ***et al***. Novel mechanisms of tumor promotion by the insulin receptor isoform a in triple-negative breast cancer cells. *Cells* 2021, 10: 3145
22. Denley, Wallace, Cosgrove, Forbes. The insulin receptor isoform exon 11-(IR-A) in cancer and other diseases: a review. *Horm Metab Res* 2003, 35: 778–785
23. Belfiore A, Malaguarnera R, Vella V, Lawrence MC, Sciacca L, Frasca F, Morrione A, ***et al***. Insulin receptor isoforms in physiology and disease: an updated view. *Endocrine Rev* 2017, 38: 379–431
24. Choi E, Duan C, Bai X. Regulation and function of insulin and insulin-like growth factor receptor signalling. *Nat Rev Mol Cell Biol* 2025, 26: 558–580
25. An W, Hall C, Li J, Hung A, Wu J, Park J, Wang L, ***et al***. Activation of the insulin receptor by insulin-like growth factor 2. *Nat Commun* 2024, 15: 2609
26. Xu Y, Margetts MB, Venugopal H, Menting JG, Kirk NS, Croll TI, Delaine C, ***et al***. How insulin-like growth factor I binds to a hybrid insulin receptor type 1 insulin-like growth factor receptor. *Structure* 2022, 30: 1098–1108.e6
27. Punjani A, Rubinstein JL, Fleet DJ, Brubaker MA. cryoSPARC: algorithms for rapid unsupervised cryo-EM structure determination. *Nat Methods* 2017, 14: 290–296
28. Punjani A, Zhang H, Fleet DJ. Non-uniform refinement: adaptive regularization improves single-particle cryo-EM reconstruction. *Nat Methods* 2020, 17: 1214–1221
29. Rosenthal PB, Henderson R. Optimal determination of particle orientation, absolute hand, and contrast loss in single-particle electron cryomicroscopy. *J Mol Biol* 2003, 333: 721–745
30. Goddard TD, Brilliant AA, Skillman TL, Vergenz S, Tyrwhitt-Drake J, Meng EC, Ferrin TE. Molecular visualization on the holodeck. *J Mol Biol* 2018, 430: 3982–3996
31. Jumper J, Evans R, Pritzel A, Green T, Figurnov M, Ronneberger O, Tunyasuvunakool K, ***et al***. Highly accurate protein structure prediction with AlphaFold. *Nature* 2021, 596: 583–589
32. Emsley P, Lohkamp B, Scott WG, Cowtan K. Features and development of *Coot*. *Acta Crystlogr D Biol Crystlogr* 2010, 66: 486–501
33. Liebschner D, Afonine PV, Baker ML, Bunkóczi G, Chen VB, Croll TI, Hintze B, ***et al***. Macromolecular structure determination using X-rays, neutrons and electrons: recent developments in *Phenix*. *Acta Crystlogr D Struct Biol* 2019, 75: 861–877
34. Nielsen J, Brandt J, Boesen T, Hummelshøj T, Slaaby R, Schluckebier G, Nissen P. Structural investigations of full-length insulin receptor dynamics and signalling. *J Mol Biol* 2022, 434: 167458
35. Viola CM, Frittmann O, Jenkins HT, Shafi T, De Meyts P, Brzozowski AM. Structural conservation of insulin/IGF signalling axis at the insulin receptors level in Drosophila and humans. *Nat Commun* 2023, 14: 6271
36. Chen Y, Chen Z, Zhao L, Li S, Ying Z, Yu P, Yan H, ***et al***. Real-time artificial intelligence assisted insulin dosage titration system for glucose control in type 2 diabetic patients: a proof of concept study. *Curr Med* 2023, 2: s44194-023-00020-7
37. De Meyts P. Insulin/receptor binding: the last piece of the puzzle? *BioEssays* 2015, 37: 389–397